Molecular dynamics simulations of a fibrillogenic peptide derived from apolipoprotein C-II

F. Sue Legge [a], Herbert Treutlein [b], Geoffrey J. Howlett [c], Irene Yarovsky [a],*

[a] *Applied Physics, School of Applied Sciences, RMIT University, GPO Box 2476V Melbourne, Victoria, 3001, Australia*
[b] *Cytopia Research Pty. Ltd., PO Box 6492, St. Kilda Road Central Melbourne, Victoria, 8008, Australia*
[c] *Biochemistry and Molecular Biology and Bio21 Molecular Science and Biotechnology Institute, University of Melbourne, Melbourne, Victoria, 3052, Australia*

Abstract

The pathway to amyloid fibril formation in proteins involves specific structural changes leading to the combination of misfolded intermediates into oligomeric assemblies. Recent NMR studies showed the presence of "turns" in amyloid peptides, indicating that turn formation may play an important role in the nucleation of the intramolecular folding and possible assembly of amyloid. Fully solvated all-atom molecular dynamics simulations were used to study the structure and dynamics of the apolipoprotein C-II peptide 56 to 76, associated with the formation of amyloid fibrils. The peptide populated an ensemble of turn structures, stabilized by hydrogen bonds and hydrophobic interactions enabling the formation of a strong hydrophobic core which may provide the conditions required to initiate aggregation. Two competing mechanisms discussed in the literature were observed. This has implications in understanding the mechanism of amyloid formation in not only apoC-II and its fragments, but also in other amyloidogenic peptides.
Crown Copyright © 2007 Published by Elsevier B.V. All rights reserved.

Keywords: Apolipoprotein; Molecular dynamics; Amyloid; Turn; Fibril; Simulation

1. Introduction

The misfolding of protein and peptides is subject to regulatory control mechanisms that lead to either refolding or degradation. However, sometimes misfolded proteins will aggregate and form insoluble amyloid fibrils. These amyloid assemblies form the basis of degenerative amyloid based diseases, such as Alzheimer's disease, Parkinson's disease and variant Creutzfeldt–Jakob disease. It is widely believed that the amyloidoses share common pathogenic mechanisms which lead to protein fibril formation and deposition. Consequently, an understanding of the folding mechanism of proteins is critical in understanding the structural changes which cause amyloid diseases. There are a family of proteins that appear to be structurally and functionally unrelated, but nevertheless, undergo the same biochemical and biophysical processes to form insoluble fibril aggregates [1]. One such protein is the human plasma apolipoprotein protein C-II (apoC-II), a component of lipoproteins and a cofactor for lipoprotein lipase [2]. ApoC-II is a 79 amino acid protein, which in lipid-free conditions folds into cross-β sheet structure to form amyloid fibrils [3]. Hydrogen–deuterium exchange and NMR spectroscopy of apoC-II fibrils revealed core regions between residues 19–37 and 57–74 [4]. This was confirmed by tryptic hydrolysis of the apoC-II fibrils yielding apoC-II(56–76), which readily formed fibrils. The ability of apoC-II to form amyloid is typical of other apolipoproteins (see Hatters et al., 2002 [5] and references therein). ApoC-II is of particular interest because aggregates of apoC-II are known to be associated with human atherosclerotic plaques and the macrophage inflammatory response [6].

Traditional experimental methods have contributed to the understanding of amyloid formation, however experimental analysis has been limited by the insolubility of the amyloid assemblies. X-ray fibre diffraction and solid state NMR studies have shown that amyloid fibrils are typically composed of cross

---

Abbreviations: apo, apolipoprotein; NMR, nuclear magnetic resonance; Aβ, β-amyloid; MD, molecular dynamics; PME, particle mesh Ewald; VMD, visual molecular dynamics; PEPCAT, peptide conformational analysis tool; SASA, solvent accessible surface area; ROG$_{hyd}$, radius of gyration of the hydrophobic residues.
 * Corresponding author. Tel.: +61 3 9925 2571; fax: +61 3 9925 5290.
 E-mail address: irene.yarovsky@rmit.edu.au (I. Yarovsky).

β-structure. This structure consists of β-strands running perpendicular to the fibril axis and hydrogen bonded to form β-sheets which run parallel to the fibril axis [7,8]. Advances recently have provided insights into understanding the structure, mechanisms and disease association of amyloidogenic peptides, including atomic structures of the spine of amyloid-like fibrils [9–12]. Despite the progress which has been made in experimental work, at the atomistic level there is limited information on the insoluble aggregates and of the mechanism relating to the structural change.

Protein fibrillation involves the formation of specific partially folded intermediates, which combine until a stable oligomeric assembly is formed. The partially folded intermediates are a result of specific structural transitions. Experimental work has shown the consistent occurrence of helix-to-β-strand transitions [13–15]. This is clearly shown in the prion protein where the transition from α-helix-to-β-sheet involves a large part of the protein [13]. Other conformational changes believed to occur are random coil→α-helix and random coil→β-strand transitions [16–21]. Studies have indicated the presence of turns in amyloid peptides which are stabilized by hydrophobic and electrostatic interactions [22]. Various studies, including solid state NMR studies, also suggest the presence of turn or bend structure in amyloid fibrils [11,23,24]. It has been postulated that "turn" formation may nucleate the intramolecular folding and subsequent assembly of amyloid [25]. In fact, one recent study showed that the amount of β-turn present in the Alzheimer's associated amyloid-β peptides correlates with the potential to aggregate into fibrils [26].
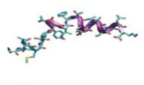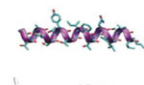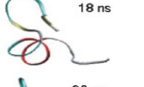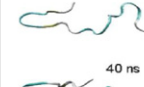
The study of β-turns and β-hairpin formation provide a good system for investigating the fundamental issues in protein folding because they are often initiation sites in early protein folding events [27,28]. The β-turn is stabilized by hydrophobic interactions, and in the case of the β-hairpin, by hydrogen bonding. The side chains move to a position to promote the formation of a hydrophobic cluster essential for the folding of the hairpin. There are different theories in the relative timing of the formation of the interstrand hydrogen bonds near the turn and the hydrophobic core. The "kinetic zipping mechanism" of Munoz hypothesized that in the folding of the hairpin [29], the β-turn forms initially thus placing the strands in a position such that the remaining hydrogen bonds are formed between the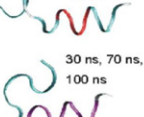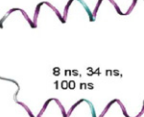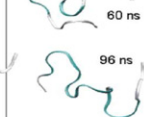 strands towards the termini regions. The turn is then further stabilized by the hydrophobic cluster formed by the aromatic residues. Alternatively, Pande [30] suggested the β-hairpin is initiated by the "hydrophobic collapse" mechanism [31], involving clustering of the hydrophobic sidechains and the subsequent formation of interstrand hydrogen bonds. The early development of the hydrophobic assembly is also discussed in a study of β-hairpin formation by Karplus [32]. This study suggests the hydrogen bonds are formed between the strands in both directions from the hydrophobic cluster. Klimov suggested the relevance of both mechanisms depending on the position of the hydrophobic cluster which in turn defines the rigidity of the hairpin [33]. The turn is likely to form first if the hydrophobic residues are located near the turn region, as in the former kinetic zipping mechanism. The latter hydrophobic collapse mechanism may be more likely when the hydrophobic residues are located in the middle of the strands such that the hydrophobic core is readily formed. On the other hand, if the hydrophobic residues are not in either position, it may be a combination of the two mechanisms.

Previous molecular dynamics (MD) studies have provided insights into the mechanism of the formation of β-turns. Bonvin simulated several starting conformations of the α-amylase inhibitor (native β-hairpin, α-left hand helical and extended conformation) over 10–30 ns at 300 K, 360 K, 400 K and observed consistent β-hairpin formation [34]. Roccatano performed simulations of protein G [35], which showed that the dynamical behaviour of the hairpin at different temperatures is very similar and large motions of the turn and end residues were observed (in agreement with experimental observations). MD has also been widely used to study the molecular properties of specific fragments of amyloidogenic proteins. The simulations have explored the mechanistic details of the fibrillation pathway and reproduced the structural transitions, including the presence of bend-motifs. These studies include simulations of single peptides [36–47] and of oligomers in various sizes and arrangements [40,48–56]. Many of these MD studies have been performed on the various peptides of the amyloid β-protein which is linked to Alzheimer's disease [41,42,44,49,57]. Conformational analysis of the Aβ(21–30) fragment, believed to be the nucleation site, have reproduced native conformations, including a bend-motif [38,42]. β-hairpins were also observed in simulations of the Aβ(25–35) fragment in water [41]. Simulations of the Aβ(1–42) fragment suggests the location of β-conformation seeding residues [58]. A conformational template identifying alternating β-bend/α-helix structure has shown the presence of a reoccurring bend-like motif in the amyloid-β peptide which would enable efficient folding of the strands of the β-sheet forming the fibrils [43]. The role of different structural elements of the Aβ(9–40) fragment, including the turn regions and the importance of hydrophobic packing in stabilizing the amyloid structure, has been investigated by Hummer [55,56]. The stability and dynamics of the prion protein has also been widely studied by MD. Conformational changes between α-helices and β-strand conformation including β-hairpin have been observed [46,54,59–61]. The presence of β-hairpins in the fibrillogenic process strongly suggests a role in the protein folding nucleation sites [62].

It is believed that small fragments of amyloidogenic proteins are integral in forming the partially folded intermediates of the fibrillation process [63,64] and that these fragments contain core regions which play a key role in aggregation [40,63,64] In our current study all-atom MD simulations have been used to investigate the dynamics of a tryptic peptide, apoC-II (56–76), derived from apoC-II for a total of 400 ns. The 56–76 peptide was chosen for study because it also has been shown experimentally to form fibrils and is believed to contain the core residues initiating the conformational change [4]. Several initial peptide conformations containing secondary structure elements associated with the structural transitions observed in fibrils were used for the MD study. Initial structures forming an α-helix, an extended strand and a β-strand as well as the experimental NMR structure of apoC-II in lipids were used. As a result 4 trajectories with the simulation time of 100 ns for each system have been generated thereby enabling us to observe the dynamical behaviour of the apoC-II peptide over a longer time period sampling different

Table 1
Snapshots of structures taken at various times during the simulation of each
system

lipid	α-helix	x-strand	β-strand
300 K	300 K	300 K	300 K
100 ns	100 ns	100 ns	100 ns

Magenta denotes α-helix, red denoted π-helix, cyan denotes turn, white denotes
coil, tan denotes bridge.

regions of the conformational space. Our simulations revealed the
presence of turn-like structure, indicating a potential role of this
region of apoC-II in the formation of amyloid structures.

2. Methods

All simulations were performed with the NAMD software
package [65] and the all-atom CHARMM27 force field [66]. The
model used in the simulations was the tryptic peptide residues 56
to 76 of apoC-II. Simulations of the fully solvated peptide in four
different starting conformations were performed: the NMR
experimental structure in dodecyl phosphocholine (PDB code:
1soh.pdb) [67] and the peptide with ideal α-helical, β-strand and
extended structures. Protonation of sidechains was consistent with
pH 7. The peptides were soaked with ∼11,800 TIP3 water
molecules [68] with density of 1 g/cm^3 in a periodic box of sizes
70 Å × 70 Å × 70 Å and 100 Å × 60 Å × 60 Å, depending on the
starting conformation. The systems were minimized by conjugate
gradient method for 1000 steps to remove steric clashes. All of the
systems were equilibrated by slow heating with temperature
reassignment to 300 K (over 24 ps) and to a total of 50 ps. During
the data collection of 100 ns for each system, the dynamics were
coupled to a temperature bath of 300 K. The atomic coordinates
were saved every 2500 steps (5 ps) for analysis. Atom-based
cutoff of 12 Å and 14 Å (depending on the system) with switching
at 10 Å was used for nonbonded interactions. The Particle Mesh
Ewald (PME) summation [69] was applied to correct for long
range electrostatic interactions. Bonds containing hydrogen atoms
were constrained using the SHAKE algorithm to their energy
minimized values, thus allowing a numerical integration time step
of 2 fs to be used in the simulation.

The four systems of apoC-II (56-76) were labelled according to
their initial structure in the following manner: *lipid* (conformation
observed in the NMR structure), *α-helix* (ideal "α-helical"
conformation), *x-strand* (ideal extended strand) and *β-strand*
(ideal "β-strand" conformation). The ideal conformations of the
α-helix, extended strand and β-strand were generated using
Pymol [70]. Details of the simulations are summarized in Table 1.
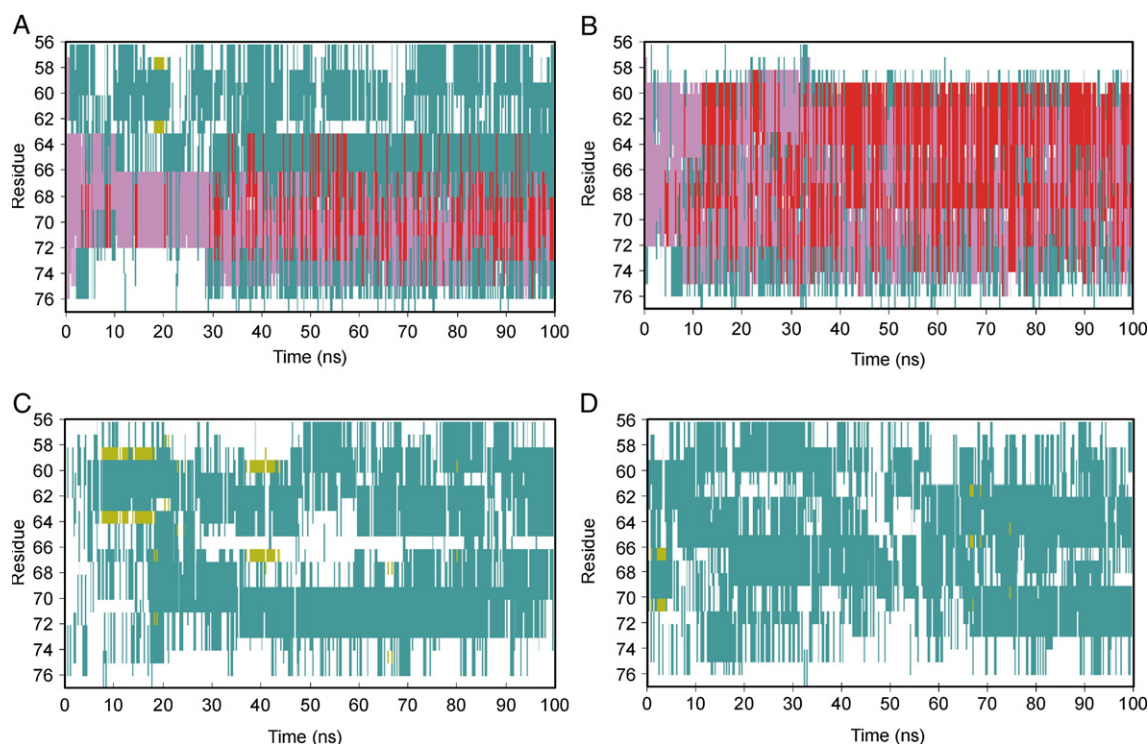

Fig. 1. Evolution of secondary structure over time for all systems of apoC-II(56–76). A. *Lipid* system. B. *α-helix* system. C. *X-Strand* system. D. *β-Strand* system.
Magenta denotes α-helix, red denoted π-helix, cyan denotes turn, white denotes coil, tan denotes bridge.

3. Results

3.1. Dynamics of the simulated structures

Table 1 shows the four starting structures and also a range of snapshots taken over the simulation. These snapshots were selected to demonstrate the results of typical changes in structure which occurred in each system and maybe referred to in the subsequent analysis and discussion. It can be seen that the *lipid* and the *α-helix* systems both retained, to different degrees, some of their helical secondary structure and also showed flexibility in the N terminal region. In the *lipid* system there was an initial loss in helical content and considerable movement of the N terminus. However, by 30 ns the structure stabilized with a largely reformed helix although with movement of the N terminus. By 70 ns a stable conformation was formed whereby the N terminus was lying in close proximity to the helix. In the *α-helix* system most of the helical content was retained, although there was some movement in the N terminus. The *x-strand* and *β-strand* systems explored a much wider region of conformational space, with regions of alternating turn structure.

3.2. Secondary structure

The evolution of the secondary structure as a function of time was determined using the STRIDE algorithm [71], as implemented in VMD [72]. The secondary structure evolution for the four

systems is shown in Fig. 1 and can be compared with the snapshots of the structures in Table 1. Fig. 2 shows the percentage of secondary structure assigned to each residue in the peptide over the simulation time course.

Examination of the secondary structure of the *lipid* system (Fig. 1A) revealed conformational changes which occurred during the simulation. During the first 30 ns of the simulation, the peptide was quite mobile and underwent considerable structural rearrangement. Between 3 and 12 ns much of the helical region of both the N and C termini regions was lost, with only residues 66 to 71 retaining their helical content as they continue to do so for the rest of the simulation. In addition, we observed turn structure centered on Met 60. At ~18 ns, a bridge occurred between Thr 57 and Thr 62. In this study, a bridge was defined as consisting of two hydrogen bonds between the adjacent residues to the bridging residues, effectively forming a β-turn. In this case the hydrogen bonds were between Ala 58–Ser 61, and Ser 56–Tyr 63, with Met 60 at the apex of the turn. A snapshot of the structure including the sidechains of the turn region is shown in Fig. 3A. In Fig. 3B, the hydrophobic residues of the turn region are represented by their van der Waals surfaces showing the hydrophobic cluster which formed close to the turn. At ~30 ns a distinct structural transition occurred, where there was a relative stabilization in the secondary structure. Between residues 66 to 75 (and to a lesser degree between residues 63–65), there was persistent fluctuation between α- and π-helix, which was present for the rest of the simulation, however, the N terminus continued to show some rearrangement
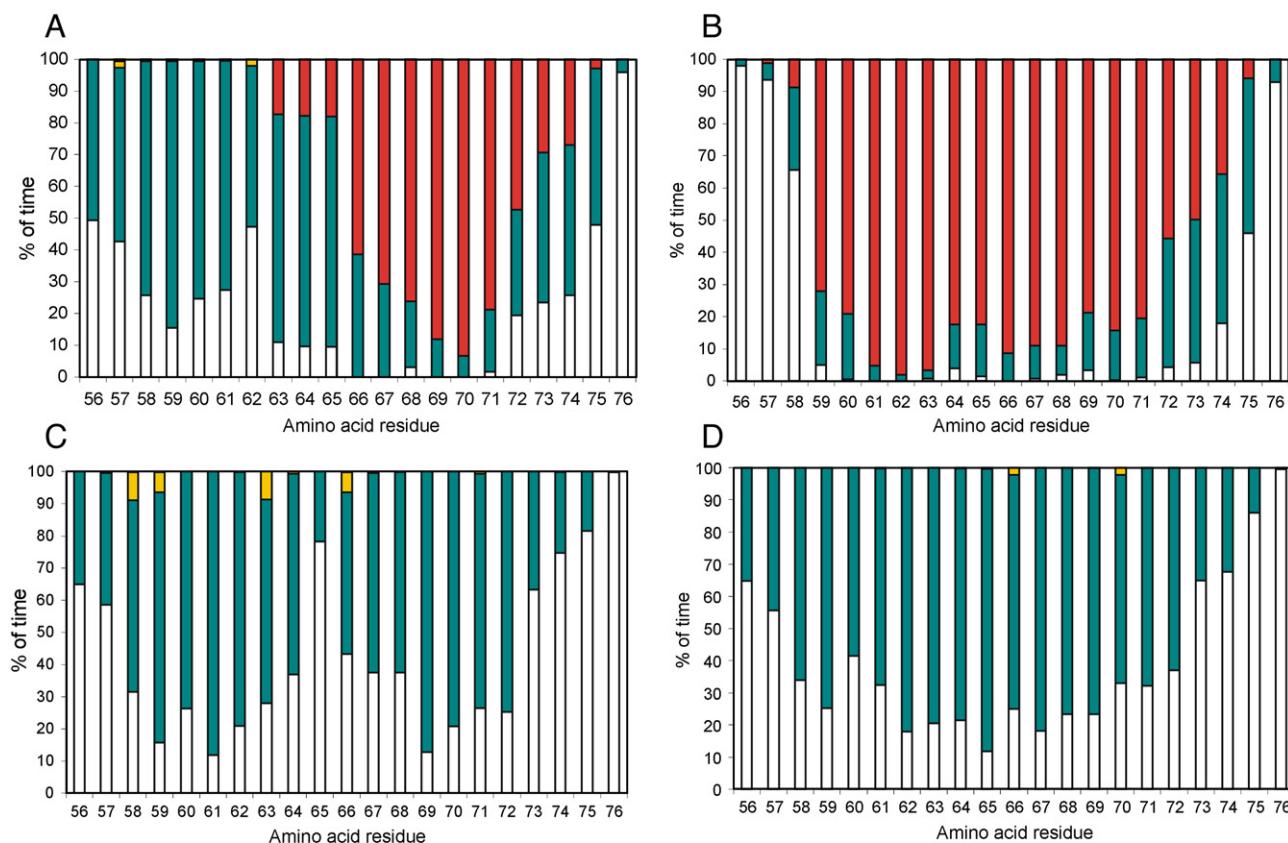

Fig. 2. Percentage of secondary structure content over time per residue for all systems of apoC-II (56–76). A. *Lipid* system. B. *α-Helix* system. C. *X-Strand* system. D. *β-Strand* system. Red denotes helix, cyan denotes turn, white denotes coil, tan denotes bridge.
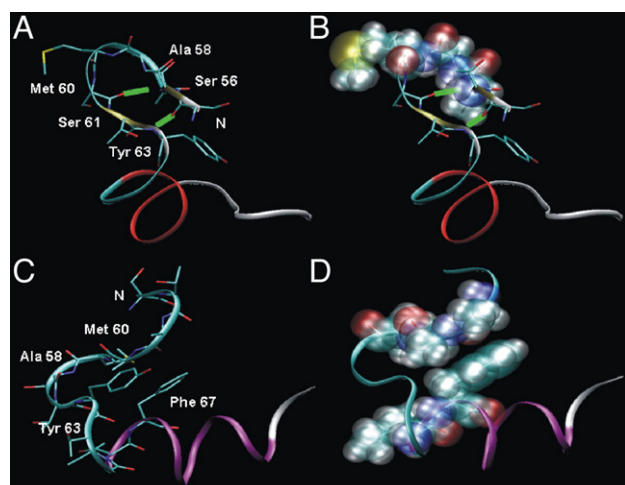
Fig. 3. Ribbon representations in the *lipid* system of bridge and turn regions of apoC-II (56–76). The two views of each turn show the sidechains represented as stick and hydrophobic sidechains as van der Waals surfaces. A, B. Bridge formed at ∼18 ns between Thr 57 and Thr 62 consisting of hydrogen bonds between Ala 58–Ser 61, and Ser 56–Tyr 63 are shown. C, D. Snapshot of turn structure at ∼70 ns. Hydrogen bonds are shown in green.

up to ∼70 ns. It has been suggested that the formation of π-helix under MD conditions may be an artifact of the specific forcefield applied to a simulation with implicit solvent [73]. As discussed in our previous work [74], an implicit solvent simulation cannot be necessarily compared to simulations in explicit solvent, such as ours. Moreover, recently it has been reported in a survey of structures from the Protein Data Bank, that the π-helix is >10 times more prevalent than previously believed depending on the type of definition algorithm of helical structure applied [75]. Transitions between α- and π-helix have been previously observed in MD simulations and are believed to be genuine physical transitions and an important stage in the helix-to-coil transition [76]. A snapshot of the structure at 70 ns is shown in Fig. 3C and D illustrates how the hydrophobic residues around Ala 58 and Phe 67 are clustered together to form a hydrophobic core. Fig. 2A shows the highly conserved helical region between residues 66 and 71, and the strong tendency to form a turn region centred on residues 59 and 60, with a bridge between residues 57 and 62.

The α-helix system (Fig. 1B) showed the most consistent stability in secondary structure over the simulated timeframe. In the first ∼8 ns the structure was mostly α-helical with some helical loss at the C terminus. After this stage, the structure was largely stable with transitions between α- and π-helix, although there was a time period between about 20 ns to 35 ns where the N terminus became more helical. The strongly conserved helical content during this simulation is illustrated in Fig. 2B. Snapshots of these structures are shown in Table 1.

In the *x-strand* system (Fig. 1C), a prevalence of turn and bridge regions were observed. The two most interesting features were the turn and bridge structure which occurred between 8 ns and 18 ns, and also between 35 ns and 40 ns. Fig. 4 illustrates the turn structures for these two bridges. Fig. 4A, B shows the turn formed at ∼8 ns. The cluster of hydrophobic residues was similar to that observed in the turn formed in the *lipid* system with the

hydrophobic residues grouped near the turn (Fig. 3A, B). Met 60 was located close to the apex of the turn as in the *lipid* system, and hydrogen bonds form between Thr 57–Thr 64 and Ala 59–Thr 62. Fig. 4C, D shows the turn formed at ∼40 ns. In this case the turn has shifted slightly away from the N terminus with Tyr 63 now at the apex of the turn. The hydrophobic residues from the two strands, including Ala 58 and Phe 67, are clustered together forming a distinct hydrophobic core, with hydrogen bonds between Ala 58–Thr 67, and Met 60–Gly 65. This turn structure was also observed just after 90 ns (Table 1). Transitory bridges were also formed at ∼18 ns (between residues 66 and 71) and ∼25 ns (between residues 59 and 64). Fig. 2C illustrates the high turn content in this system, including the bridge formation observed between residues 58 to 63, and 59 to 66.

The secondary structure of the last system, the *β-strand* system (Fig. 1D), showed a predominance of turn structure forming, with the brief appearance of a bridge early in the simulation at ∼3–4 ns. This turn is shown in Fig. 5A, B with hydrophobic residues around Ile 66 clustered towards the turn region, and hydrogen bonds between Gly 65–Val 71 and Phe 67–Asp 69. The peptide
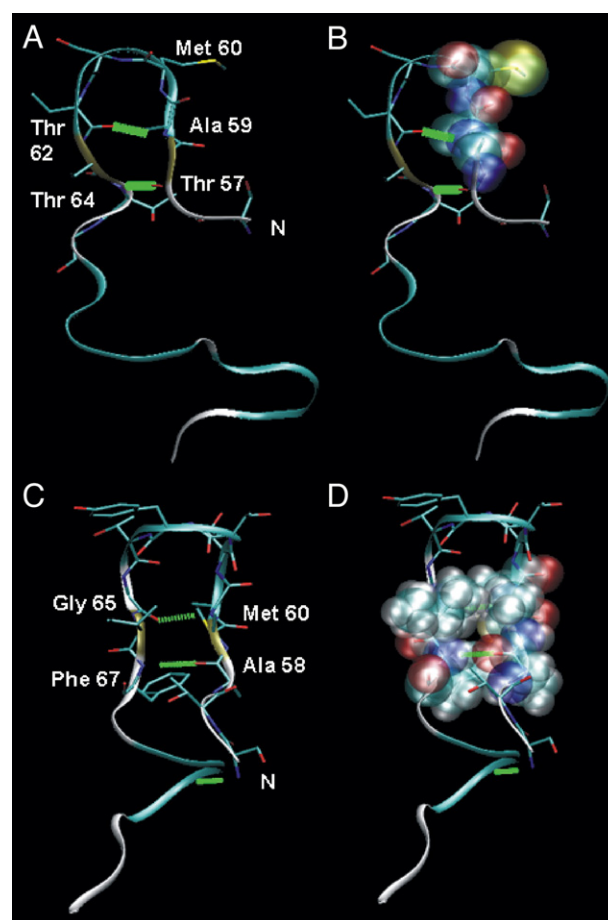
Fig. 4. Ribbon representations in the *x-strand* system of turn and bridge regions of apoC-II (56–76). The two views of each turn show the sidechains represented as stick and hydrophobic sidechains as van der Waals surfaces. A, B. Bridge formed at ∼8 ns between Ala 58 and Tyr 63 consisting of hydrogen bonds between Thr 57–Thr 64 and Ala 59–Thr 62. C, D. Bridge formed at ∼40 ns between Ala 59 and Ile 66 consisting of hydrogen bonds between Ala 58–Thr 67, and Met 60–Gly 65. Hydrogen bonds are shown in green.
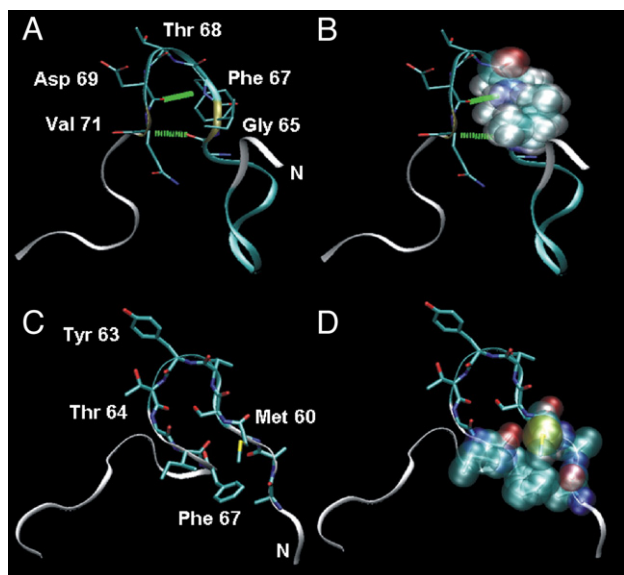
Fig. 5. Ribbon representation of turn and bridge regions in *β-strand* system of apoC-II (56–76). The two views of each turn show the sidechains represented as stick and hydrophobic sidechains as van der Waals surfaces. A, B. Bridge formed at ~4 ns between Ile 66 and Glu 70 consisting of hydrogen bonds between Gly 65–Val 71 and Phe 67–Asp 69. C, D. Turn formed at ~60 ns centered on Tyr 63. Hydrogen bonds are shown in green.

continued to undergo rearrangement, with some reasonably stable turn structure formed by ~20 ns centred on Ala 58 and Phe 67. At ~40 ns, there was poor secondary structure definition, reflecting disorder in the system. Between 60 ns and 65 ns the peptide formed a turn centred on Tyr 63 which was stabilized by transient bridge structure, and was maintained nearly to the end of the simulation (Fig. 5C,D). This structure was similar in conformation to that observed in the *x-strand* system at ~40 ns, with a hydrophobic core formed at the base of the turn, which included residues Ala 58 and Phe 67. The high content of the turn structure in this system is shown in Fig. 2D.

3.3. Cluster analysis

A cluster analysis was performed to further characterize the conformational states of apoC-II (56–76) generated during the simulations. The program PEPCAT [77] (PEPtide Conformational Analysis Tool) was used to classify the structures according to a large set of geometric descriptors. The descriptors were based on the following definition of a β-turn: Cαn to Cαn+3 distance <7 Å and the structure is not helical [78–81]. The helix was described as Cαn to Cαn+4 distance >7 Å. This resulted in 35 geometric descriptors to describe the 20 residue peptide. Although, this fairly rigid definition classified the structures into a large number of conformational states, it provided useful information about the conformational transitions by resolving subtle structural changes.

Fig. 6 shows the evolution of the conformational states which occurred over the simulation time course. The plot provides information about the peptide dynamics — the gradient indicates the degree of structural change and the clusters of conformational states indicate the transition to a relatively stable set of like-conformations (it should be noted that in the interest of clarity,

different scales were used on the y-axis). As expected a large number of states were observed for all systems.

In the *lipid* system (Fig. 6) approximately 2800 conformational states were observed. Up to ~30 ns, the relatively steep gradient of the plot reflected the increased mobility of the structure, with many conformational states defined. At ~30 ns, although there were still some new conformational states occurring; the simulation largely stabilized into a small number of well populated states for the remaining simulation time. This trend was in agreement with the secondary structure analysis for this system where a distinct transition was observed at ~30 ns (Fig. 1A). The most frequently occupied states, States 1838 and 1781, were formed at this time period and the plot shows that the structure of the peptide underwent a frequent transition between these two states. These states formed a part of a distinct set of conformational states between States 1750 and 2000 which were similar in structure, and varied by only a few geometric descriptors in the N terminal region. Representative structures of States 1838 and 1781 are shown in Fig. 6A (these structures correspond to the last two snapshots in Table 1 for this system), including like-conformational states, and altogether accounted for residency time of 23.1 ns and 6.8 ns, respectively. The structures were very similar, except for the flexibility in the N terminus which was either lying close to, or away from the helix. A closer inspection of the plot revealed the fluctuations between the two states occurred until ~70 ns where the structure left the transition State 1750 and assumed State 1838. This event corresponded to the stabilization of the N terminus observed in the secondary structure at this time point. State 1838 is the same conformation as that shown in Fig. 3C, D.

The cluster analysis of the *α-helix* system produced the lowest number of conformational states ~665 (Fig. 6B), which correlated with the stability observed in the secondary structure analysis of this system (Fig. 1B). The plot shows a stabilization of structure at ~8 ns, when the most populated states occurred (States 382 and 482). There were frequent transitions between these states for the remainder of the simulation, with the exception of a brief period (20–35 ns), when the N terminus refolded into helical form (State 509). These conformations are shown in Fig. 6B and can be compared to those in Table 1. The structures showed some similarity to those observed in the previous system, although in this system the N terminus was less variable, thus forming a unique set of conformational states. Overall, it would appear that the initial starting structure was in a deep energy well, and an energy barrier needed to be overcome for a significant conformational transition to occur.

The *x-strand* system showed greater variability with ~5363 conformational states (Fig. 6C). A distinct cluster of conformational states was observed forming at ~35 ns, and to a lesser degree at ~8 ns, ~25 ns, ~50 ns and ~90 ns with periods of greater flexibility between. These clusters largely corresponded to the formation of the bridges observed at ~8 ns and ~35 ns and the turn region formed at ~90 ns in the secondary structure (Fig. 1C). Each of these three clusters consisted of a large number of like-conformational states, accounting for a residency time of approximately 9 ns, 7 ns and 8 ns, respectively. Structures of some of the most populated states of these clusters are shown in
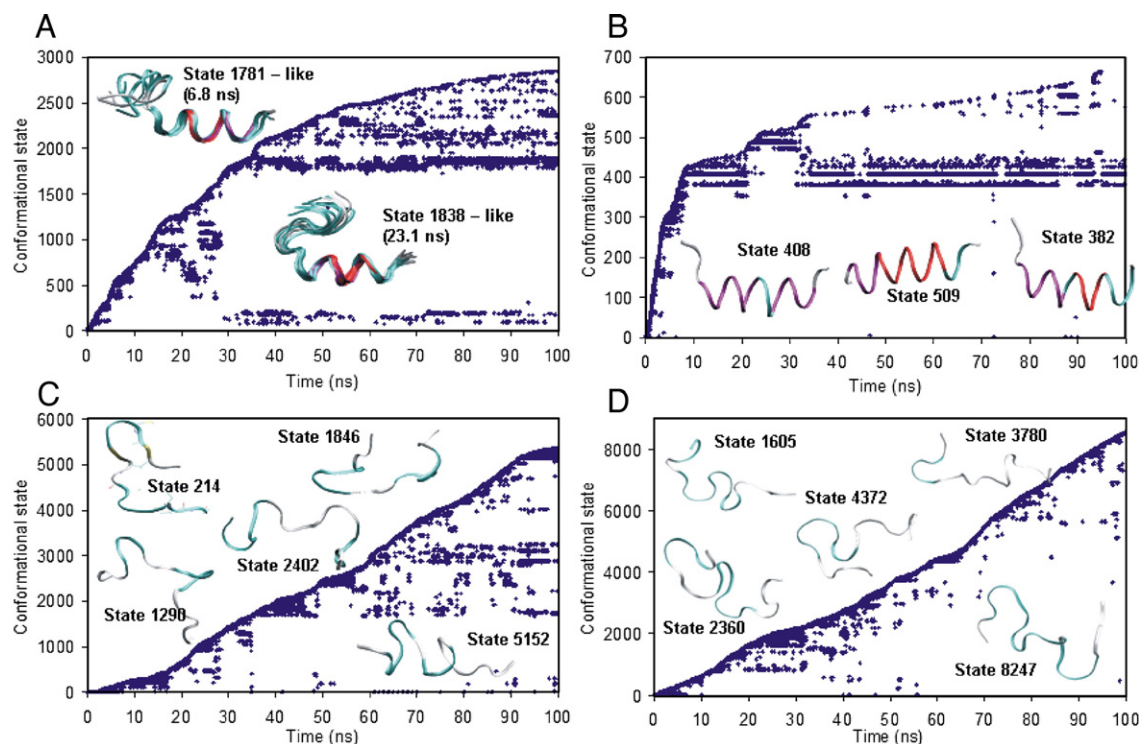
Fig. 6. Cluster analysis: evolution of conformational states over time for all systems of apoC-II (56–76). A. *Lipid* system. B. *α-Helix* system. C. *X-Strand* system. D. *β-Strand* system. The nature of the plot provides information regarding the flexibility and distinct changes in structure (for clarity, different scales are used on the y-axis).

Fig. 6C, and it is interesting to note that the turn region at ~35 ns and the turn region formed at ~90 ns are in a similar location in the peptide.

The *β-strand* system showed the most variability with nearly 8600 conformational states observed (Fig. 6D). The plot shows some clustering of the conformational states over the simulation time. For example, clustering was observed early in the simulation between 0–5 ns, and also at 20 ns and 60 ns. This correlates with the secondary structure observed — the bridge at ~3–4 ns (Fig. 1D), and the formation of turn structure at 20 ns and 60 ns.

3.4. Solvent accessible surface area

The previous analysis of the simulations revealed that the *lipid* and *x-strand* systems (and to a lesser extent the *β-strand* system) formed similar types of turn structure characterized by hydrophobic patches or clusters. The turn region formed, firstly with Met 60 at the apex, and then moved away in sequence from the N terminus to form a turn with apex at Tyr 63. The hydrophobic residues were initially located near the turn region. As the simulations progressed, the hydrophobic residues rearranged and clustered together to form a hydrophobic core. It is believed that hydrophobic interactions play an important role, not only in the stability of the folded states, but also drive the early stages of oligimerisation in the formation of amyloid fibrils [82]. To assess the potential contribution of the hydrophobic forces and to explore further the nature of the turn regions and the role of the individual residues, the solvent accessible surface area (SASA) was calculated for the systems. The changes in total SASA for the hydrophobic residues (Ala

58, Ala 59, Met 60, Ile 66, Phe 67, Val 71, Leu 72, Val 74, Leu 75) of each peptide over the simulation time are shown in Fig. 7A. The plot shows a moving average of 250 ps. To

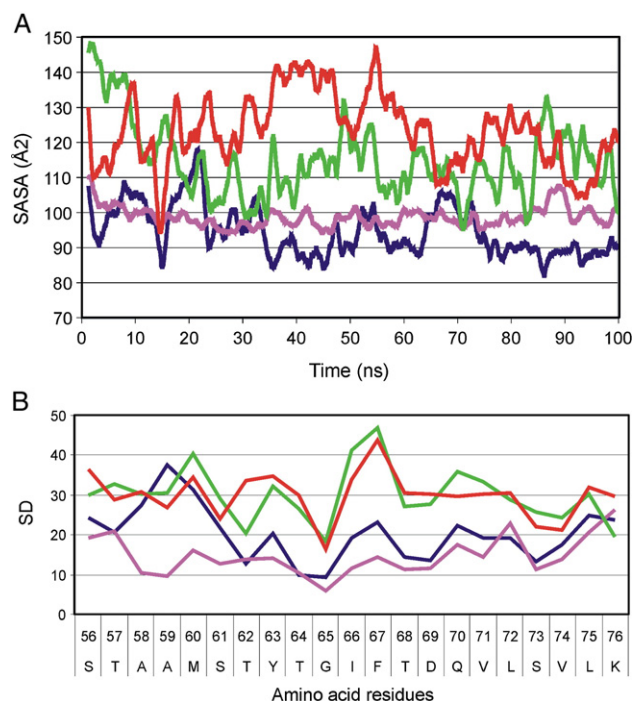
Fig. 7. SASA of apoC-II(56–76) for the *lipid* (blue), *α-helix* (magenta), *x-strand* (green) and *β-strand* (red) systems. A. Changes in total SASA of the hydrophobic residues in the peptides over the simulation time course. The plot shows a moving average of 250 ps. B. Variation (standard deviation) in the SASA of each residue averaged over the simulation time.

characterize the changes occurring in the SASA, the variation of the SASA for each residue averaged over the simulation time for each system are shown in Fig. 7B.

The *lipid* system generally showed the lowest SASA of the four systems, although fluctuations occurred particularly in the first 30 ns (Fig. 7A). A peak occurred at ~20 ns, just after the formation of the bridge at ~18 ns (Fig. 3), characterized by the hydrophobic residues clustered near the turn region and thus solvent exposed. The SASA then decreased, although still undergoing some fluctuations. By ~70 ns the SASA was stabilized, corresponding to the persistent formation of the hydrophobic core observed at this time frame. Fig. 7B monitors the variation in SASA of the individual residues and overall, the hydrophobic residues generally showed a large fluctuation. The largest variation in SASA occurred in the hydrophobic residues Ala58, Ala59, and Met60. The snapshot of the structure shown in Fig. 3C, D, which was stabilized by ~70 ns, was the most frequented conformation (State 1838). The hydrophobic residues 58–60 interacted with Phe 67 to form a strong hydrophobic core thus stabilizing both the N terminus and the helical region. This hydrophobic core is of the type proposed to be a potential starting point for aggregation.

The SASA values of the hydrophobic residues of the *α-helix* system showed the greatest constancy, which was not surprising given the stability of this system. There was little fluctuation in the SASA of the hydrophobic residues (Fig. 7A). This was most evident in the variation of the residues Ala58, Ala59, and Met60 (Fig. 7B), when compared to the same residues in the previous system.

The SASA values of the hydrophobic residues in the *x-strand* system (Fig. 7A) was higher than that of the *lipid* system, although there were some similarities in the trend. With the appearance of the bridge at 8 ns characterized by hydrophobic residues exposed near the turn region (Fig. 4A, B), the SASA was relatively high. However, by the time the second bridge had formed at ~40 ns (Fig. 4C, D), the SASA had decreased, and although there were fluctuations corresponding to rearrangements in structure, the SASA generally stayed at this level. This bridge structure formed a hydrophobic core similar to that observed in the *lipid* system. The variation in SASA of this system (Fig. 7B) showed a similar pattern of values to the *lipid* system in the N terminal region (approximately residue 56 to 65), however, the C terminal region showed a higher SASA and greater variation, particularly for the hydrophobic residues. This is probably a reflection of the lower amount of helix in this region and the less ordered C-terminal region. Interestingly, the highest fluctuation occurred in Met 60, Ile 66 and Phe 67, residues involved in the formation of the hydrophobic core.

In the last system, *β-strand*, the SASA of the hydrophobic residues showed the most changes in values (Fig. 7A), although by 65 ns some decrease in values were observed. This is probably related to the formation of the turn structure at ~60 ns characterized by the hydrophobic residues forming a hydrophobic core. The variation in SASA for each residue was similar to that of the *x-strand* system (Fig. 7B), with the highest fluctuation occurring in the Met 60, Ile 66 and Phe 67.
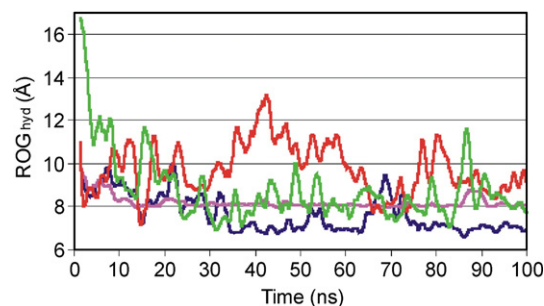

Fig. 8. Radius of gyration of the hydrophobic residues of apoC-II(56–76) for the *lipid* (blue), *α-helix* (magenta), *x-strand* (green) and *β-strand* (red) systems. The plot shows a moving average of 250 ps.

3.5. Radius of gyration

The radius of gyration of the hydrophobic residues Ala 58, Ala 59, Met 60, Ile 66, Phe 67, Val 71, Leu 72, Val 74, Leu 75 (ROG$_{hyd}$) was calculated as an indication of the presence of the hydrophobic core. Fig. 8 shows the ROG$_{hyd}$ for each system. The plot shows a moving average of 250 ps. Overall the ROG$_{hyd}$ for each system showed similar trends to the SASA discussed previously. The *lipid* system showed a decrease in ROG$_{hyd}$ by ~30 ns and remained at this level (apart from a brief increase at ~70 ns), correlating with the appearance of the hydrophobic clusters. As expected, the *α-helix* system showed little variation, with values generally higher than those of the *lipid* system. The *x-strand* system showed the highest initial ROG$_{hyd}$, however, a notable decrease occurred by ~30 ns, corresponding to the time of formation of the second type of hydrophobic cluster, and largely remained at this level apart from a brief increase just before ~90 ns. The *β-strand* system showed the most flexibility, with the highest point occurring at ~40 ns. This correlates with the unstructured region observed in the secondary structure. There was a decrease at 65 ns, corresponding to the formation of the turn structure observed in the previous analysis.

4. Discussion and conclusion

Recent studies have suggested that the pre-fibrillar aggregates are considerably more toxic than the mature amyloid fibrils [83,84]. Inhibiting the folding and formation of these pathological amyloid precursors may be effective in the treatment of amyloid based diseases. Therefore, it is important to gain an understanding of the types of interactions and consequent structural changes which lead to the formation of these aggregates.

Although there was wide variety of conformations sampled in the four systems studied, a clustering of structural types was observed that illustrated the conformational transitions occurring during the simulation. Overall, the apoC-II peptide showed a strong propensity to populate an ensemble of turn-like structure. In the *lipid* system, a hydrophobic cluster formed following a mutual stabilisation of the N terminus and the helical region. This also occurred in the *x-strand* system, although there was only slight evidence of helix formation. In the *β-strand* system there was turn structure which resembled the previous two systems. We classified these turns into two types: firstly, Met 60 is located at the apex of

the turn, and the hydrophobic residues (residue 58–60) are clustered near the turn region; secondly, Tyr 63 is at the apex, and the hydrophobic residues (residues 66–67, and 58–60) are located in the middle of the two strands. As discussed in the cluster analysis, the first type of hydrophobic cluster had a residency time in the *lipid* and *x-strand* systems of 23.1 ns and ∼9 ns, respectively. The second type of hydrophobic cluster had a residency time in the *lipid* and *x-strand* systems of approximately 6.8 ns and ∼15 ns, respectively (the latter time includes the second bridge, 8 ns, and the turn region formed at the end of the simulation, 7 ns). These types of hydrophobic clusters are illustrated in the schematic in Fig. 9. Fig. 9 also shows the hydrogen bonding pattern observed in the *x-strand* system. Some variation in the hydrogen bond pattern in the turns was observed between systems, however, the position of the hydrophobic residues largely followed the types described above.

The proposed mechanism of formation of β-turn was discussed in the introduction to this paper. It was suggested that the location of the hydrophobic residues influences the relative timing of the formation of the interstrand hydrogen bonds near the turn and the hydrophobic core [33]. In our simulations we saw evidence of both mechanisms in the formation of the turn structure — in the first hydrophobic cluster formed with the hydrophobic residues located near the turn region, such that the turn is likely to form first, as in the "kinetic zipping" mechanism [29]. In the second type of hydrophobic cluster observed, we saw support for the "hydrophobic collapse" mechanism [30], where the hydrophobic residues are located in the middle of the strands such that the hydrophobic core is formed, facilitating the subsequent formation of the interstrand hydrogen bonds. The formation of the initial turn maybe a precursor step to the turn characterized by the hydrophobic core. The hydrogen bond network between the backbone atoms of the peptide associated with the bridge or turn structure does not persist throughout the simulation. Even in the *x-strand* system, where there was the greatest prevalence of hydrogen bonds associated with the bridge formation, these hydrogen bonds still only account for about 15 ns of the 100 ns simulation.

The occurrence of hydrophobic clusters in the simulation of the peptides has implications in the formation of oligomers for both types of clusters observed in our simulations. Even though there is

a strong tendency to form hydrophobic clusters, there are still fluctuations in the position of the hydrophobic residues as shown in the SASA in Fig. 7. Therefore, these clusters may present possible hydrophobic interaction sites with other peptides sharing similar structural features. As we observed, the turn formation was facilitated by both hydrophobic interactions and hydrogen bonds between the backbone atoms. However, as the internal hydrogen bonds do not persist in the dynamics of the peptide they are potentially available to hydrogen bond and form β-structure with other similar peptides — a possible nucleation mechanism of fibrillation. The importance of hydrophobic interactions in the formation of oligomers of amyloid peptides has been shown in previous MD simulations by Buchete et al. [55,56]. The authors tested the stability of oligomers of Aβ(1–40) at ambient and elevated temperatures, and showed that whilst the hydrophobic core remained intact, the loop or turn regions tend to be less stable. In our study, we observed persistent hydrophobic clusters despite a higher mobility of the turn region. The higher flexibility of the turns might allow the faster formation of the two types of clusters formed as previously discussed.

The four different starting structures of the peptide used in the simulations varied in their flexibility, as expected. The peptide exhibited stronger tendency to fold when the initial structure was in extended and β structure, with the helical starting structure showing the highest stability. This property has previously been observed in simulation studies of a β-hairpin peptide [85]. The transition between the zipping mechanism and the hydrophobic collapse methods described above was observed in the *lipid* and *x-strand* systems. The structural transitions were also observed to a lesser extent in the *β-strand* system, which may reflect the need for a longer simulation time. The *α-helix* system showed the least structural change, probably reflecting the intrinsic stability of this conformation, although overall the *lipid* system (which is the NMR structure) showed the lowest SASA reflecting the highest sidechain packing.

The total of 400 ns of simulation time is of sufficient length to reveal characteristic elements of the crucial initial stage of amyloidosis. The formation of turn structure and subsequent hydrophobic core provide the conditions to drive aggregation and fibril formation. These results suggest the importance of future analysis of different sized peptides of apoC-II, such as apoC-II (60–70). Recent experimental work has shown that the ten residue peptide of apoC-II(60–70) also forms amyloid fibrils [4], and is potentially the region which nucleates the fibrillation folding process. This peptide is contained within the apoC-II (56–76) peptide and was the region where we observed much of the turn structure. The MD simulations also provide the opportunity to investigate the dynamic behaviour of individual residues in the amyloid prone peptide, for example, Met 60 of apoC-II. The oxidation of Met is known to, not only reduce or eliminate biological activity [86–89], but is also linked with changes in the assembly of fibrils and may reduce propensity for fibril formation [90–92]. This work could be continued by performing simulations of mutant variants of the peptides to provide insights into the role of particular residues. Lastly, the turn structures obtained from the simulations will be useful starting structures to build models of possible oligomeric amyloid of apoC-II.

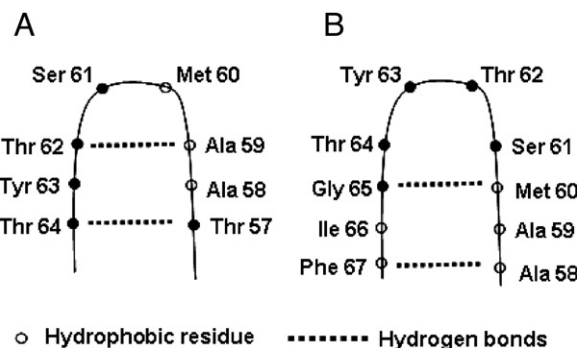Fig. 9. Schematic illustrating the two types of hydrophobic patches or clusters formed in the *lipid* and *x-strand* systems (and to a lesser extent the *β-strand* system). The hydrogen bonding network observed in the *x-strand* system is shown. A. Met 60 at apex; hydrophobic residues are clustered near the turn region. B. Tyr 63 at apex; hydrophobic residues are located in the middle of the two strands.

Acknowledgment

References

[1] P. Westermark, M.D. Benson, J.N. Buxbaum, A.S. Cohen, B. Frangione, S. Ikeda, C.L. Masters, G. Merlini, M.J. Saraiva, J.D. Sipe, Amyloid: toward terminology clarification. Report from the Nomenclature Committee of the International Society of Amyloidosis, Amyloid 12 (2005) 1–4.

[2] R.L. Jackson, G. Holdsworth, Isolation and properties of human apolipoproteins C-I, C-II, and C-III, Methods Enzymol. 128 (1986) 288–297.

[3] D.M. Hatters, C.E. MacPhee, L.J. Lawrence, W.H. Sawyer, G.J. Howlett, Human apolipoprotein C-II forms twisted amyloid ribbons and closed loops, Biochemistry 39 (2000) 8276–8283.

[4] L.M. Wilson, Y.F. Mok, K.J. Binger, M.D. Griffin, H.D. Mertens, F. Lin, J.D. Wade, P.R. Gooley, G.J. Howlett, A structural core within apolipoprotein C-II amyloid fibrils identified using hydrogen exchange and proteolysis, J. Mol. Biol. (2006).

[5] D.M. Hatters, G.J. Howlett, The structural basis for amyloid formation by plasma apolipoproteins: a review, Eur. Biophys. J. 31 (2002) 2–8.

[6] L.A. Medeiros, T. Khan, J.B. El Khoury, C.L. Pham, D.M. Hatters, G.J. Howlett, R. Lopez, K.D. O'Brien, K.J. Moore, Fibrillar amyloid protein present in atheroma activates CD36 signal transduction, J. Biol. Chem. 279 (2004) 10643–10648.

[7] M. Sunde, L.C. Serpell, M. Bartlam, P.E. Fraser, M.B. Pepys, C.C. Blake, Common core structure of amyloid fibrils by synchrotron X-ray diffraction, J. Mol. Biol. 273 (1997) 729–739.

[8] M. Sunde, C.C. Blake, From the globular to the fibrous state: protein structure and structural conversion in amyloid formation, Q. Rev. Biophys. 31 (1998) 1–39.

[9] R. Nelson, M.R. Sawaya, M. Balbirnie, A.O. Madsen, C. Riekel, R. Grothe, D. Eisenberg, Structure of the cross-beta spine of amyloid-like fibrils, Nature 435 (2005) 773–778.

[10] S.W. Liebman, Structural clues to prion mysteries, Nat. Struct. Biol. 12 (2005) 567–568.

[11] C. Ritter, M.L. Maddelein, A.B. Siemer, T. Luhrs, M. Ernst, B.H. Meier, S.J. Saupe, R. Riek, Correlation of structural elements and infectivity of the HET-s prion, Nature 435 (2005) 844–848.

[12] M.R. Sawaya, S. Sambashivan, R. Nelson, M.I. Ivanova, S.A. Sievers, M.I. Apostol, M.J. Thompson, M. Balbirnie, J.J. Wiltzius, H.T. McFarlane, A.O. Madsen, C. Riekel, D. Eisenberg, Atomic structures of amyloid cross-beta spines reveal varied steric zippers, Nature (2007).

[13] K.M. Pan, M. Baldwin, J. Nguyen, M. Gasset, A. Serban, D. Groth, I. Mehlhorn, Z. Huang, R.J. Fletterick, F.E. Cohen, et al., Conversion of alpha-helices into beta-sheets features in the formation of the scrapie prion proteins, Proc. Natl. Acad. Sci. U. S. A. 90 (1993) 10962–10966.

[14] D. Jayawickrama, S. Zink, D. Vander Velde, R.I. Effiong, C.K. Larive, Conformational analysis of the beta-amyloid peptide fragment, beta(12–28), J. Biomol. Struct. Dyn. 13 (1995) 229–244.

[15] Y. Levy, E. Hanan, B. Solomon, O.M. Becker, Helix–coil transition of PrP106–126: molecular dynamic study, Proteins 45 (2001) 382–396.

[16] C.J. Barrow, A. Yasuda, P.T. Kenny, M.G. Zagorski, Solution conformations and aggregational properties of synthetic amyloid beta-peptides of Alzheimer's disease. Analysis of circular dichroism spectra, J. Mol. Biol. 225 (1992) 1075–1093.

[17] M. Coles, W. Bicknell, A.A. Watson, D.P. Fairlie, D.J. Craik, Solution structure of amyloid beta-peptide(1–40) in a water–micelle environment. Is the membrane-spanning domain where we think it is? Biochemistry 37 (1998) 11064–11077.

[18] M.G. Zagorski, C.J. Barrow, NMR studies of amyloid beta-peptides: proton assignments, secondary structure, and mechanism of an alpha-helix–beta-sheet conversion for a homologous, 28-residue, N-terminal fragment, Biochemistry 31 (1992) 5621–5631.

[19] S. Zhang, K. Iwata, M.J. Lachenmann, J.W. Peng, S. Li, E.R. Stimson, Y. Lu, A.M. Felix, J.E. Maggio, J.P. Lee, The Alzheimer's peptide a beta adopts a collapsed coil structure in water, J. Struct. Biol. 130 (2000) 130–141.

[20] H. Shao, S. Jao, K. Ma, M.G. Zagorski, Solution structures of micelle-bound amyloid beta-(1–40) and beta-(1–42) peptides of Alzheimer's disease, J. Mol. Biol. 285 (1999) 755–773.

[21] C. Soto, E.M. Castano, B. Frangione, N.C. Inestrosa, The alpha-helical to beta-strand transition in the amino-terminal fragment of the amyloid beta-peptide modulates amyloid formation, J. Biol. Chem. 270 (1995) 3063–3067.

[22] I. Laczko, S. Holly, Z. Konya, K. Soos, J.L. Varga, M. Hollosi, B. Penke, Conformational mapping of amyloid peptides from the putative neurotoxic 25–35 region, Biochem. Biophys. Res. Commun. 205 (1994) 120–126.

[23] A.T. Petkova, Y. Ishii, J.J. Balbach, O.N. Antzutkin, R.D. Leapman, F. Delaglio, R. Tycko, A structural model for Alzheimer's beta-amyloid fibrils based on experimental constraints from solid state NMR, Proc. Natl. Acad. Sci. U. S. A. 99 (2002) 16742–16747.

[24] T. Luhrs, C. Ritter, M. Adrian, D. Riek-Loher, B. Bohrmann, H. Dobeli, D. Schubert, R. Riek, 3D structure of Alzheimer's amyloid-beta(1–42) fibrils, Proc. Natl. Acad. Sci. U. S. A. 102 (2005) 17342–17347.

[25] N.D. Lazo, M.A. Grant, M.C. Condron, A.C. Rigby, D.B. Teplow, On the nucleation of amyloid beta-protein monomer folding, Protein Sci. 14 (2005) 1581–1596.

[26] S. Hashioka, A. Monji, T. Ueda, S. Kanba, H. Nakanishi, Amyloid-beta fibril formation is not necessarily required for microglial activation by the peptides, Neurochem. Int. 47 (2005) 369–376.

[27] F. Blanco, M. Ramirez-Alvarado, L. Serrano, Formation and stability of beta-hairpin structures in polypeptides, Curr. Opin. Struct. Biol. 8 (1998) 107–111.

[28] M. Ramirez-Alvarado, F.J. Blanco, L. Serrano, De novo design and structural analysis of a model beta-hairpin peptide system, Nat. Struct. Biol. 3 (1996) 604–612.

[29] V. Munoz, P.A. Thompson, J. Hofrichter, W.A. Eaton, Folding dynamics and mechanism of beta-hairpin formation, Nature 390 (1997) 196–199.

[30] V.S. Pande, D.S. Rohksar, Molecular dynamics simulations of unfolding and refolding of a β-hairpin fragment of protein G, Proc. Natl. Acad. Sci. U. S. A. 96 (1999) 9062–9067.

[31] C. Tanford, The Hydrophobic Effect, Wiley, New York, 1980.

[32] A.R. Dinner, T. Lazaridis, M. Karplus, Understanding beta-hairpin formation, Proc. Natl. Acad. Sci. U. S. A. 96 (1999) 9068–9073.

[33] D.K. Klimov, D. Thirumalai, Mechanisms and kinetics of beta-hairpin formation, Proc. Natl. Acad. Sci. U. S. A. 97 (2000) 2544–2549.

[34] A.M. Bonvin, W.F. van Gunsteren, beta-Hairpin stability and folding: molecular dynamics studies of the first beta-hairpin of tendamistat, J. Mol. Biol. 296 (2000) 255–268.

[35] D. Roccatano, A. Amadei, A. Di Nola, H.J. Berendsen, A molecular dynamics study of the 41–56 beta-hairpin from B1 domain of protein G, Protein Sci. 8 (1999) 2130–2143.

[36] F. Simona, G. Tiana, R.A. Broglia, G. Colombo, Modeling the alpha-helix to beta-hairpin transition mechanism and the formation of oligomeric aggregates of the fibrillogenic peptide Abeta(12–28): insights from all-atom molecular dynamics simulations, J. Mol. Graph. Model. 23 (2004) 263–273.

[37] Z.Y. Guo, S. Wang, Y.H. Tang, Y.M. Feng, Mutagenesis of the three conserved valine residues: consequence on the foldability of insulin, Biochim. Biophys. Acta 1699 (2004) 103–109.

[38] J.M. Borreguero, B. Urbanc, N.D. Lazo, S.V. Buldyrev, D.B. Teplow, H.E. Stanley, Folding events in the 21–30 region of amyloid beta-protein (Abeta) studied in silico, Proc. Natl. Acad. Sci. U. S. A. 102 (2005) 6015–6020.

[39] L. Cruz, B. Urbanc, J.M. Borreguero, N.D. Lazo, D.B. Teplow, H.E. Stanley, Solvent and mutation effects on the nucleation of amyloid beta-protein folding, Proc. Natl. Acad. Sci. U. S. A. 102 (2005) 18258–18263.

[40] G. Colombo, I. Daidone, E. Gazit, A. Amadei, A. Di Nola, Molecular dynamics simulation of the aggregation of the core-recognition motif of the islet amyloid polypeptide in explicit water, Proteins 59 (2005) 519–527.

[41] G. Wei, J.E. Shea, Effects of solvent on the structure of the Alzheimer amyloid-{beta}(25–35) peptide, Biophys. J. (2006).

[42] A. Baumketner, S.L. Bernstein, T. Wyttenbach, N.D. Lazo, D.B. Teplow, M.T. Bowers, J.E. Shea, Structure of the 21–30 fragment of amyloid beta-protein, Protein Sci. 15 (2006) 1239–1247.

[43] D. Zanuy, K. Gunasekaran, A.M. Lesk, R. Nussinov, Computational study of the fibril organization of polyglutamine repeats reveals a common motif identified in beta-helices, J. Mol. Biol. 358 (2006) 330–345.

[44] B. Ma, R. Nussinov, The stability of monomeric intermediates controls amyloid formation: A{beta}25–35 and its N27Q mutant, Biophys. J. 90 (2006) 3365–3374.

[45] M.F. Yang, M. Lei, B. Yordanov, S.H. Huo, Peptide plane can flip in two opposite directions: implication in amyloid formation of transthyretin, J. Phys. Chem., B 110 (2006) 5829–5833.

[46] J. Zheng, B. Ma, C.J. Tsai, R. Nussinov, Structural stability and dynamics of an amyloid-forming peptide GNNQQNY from the yeast prion Sup-35, Biophys. J. (2006).

[47] J. Lipfert, J. Franklin, F. Wu, S. Doniach, Protein misfolding and amyloid formation for the peptide GNNQQNY from yeast prion protein Sup35: simulation by reaction path annealing, J. Mol. Biol. 349 (2005) 648–658.

[48] H. Lei, C. Wu, Z. Wang, Y. Duan, Molecular dynamics simulations and free energy analyses on the dimer formation of an amyloidogenic heptapeptide from human beta2-microglobulin: implication for the protofibril structure, J. Mol. Biol. 356 (2006) 1049–1063.

[49] M. Cecchini, R. Curcio, M. Pappalardo, R. Melki, A. Caflisch, A molecular dynamics approach to the structural characterization of amyloid aggregation, J. Mol. Biol. 357 (2006) 1306–1321.

[50] P. Soto, J. Cladera, A.E. Mark, X. Daura, Stability of SIV gp32 fusion-peptide single-layer protofibrils as monitored by molecular-dynamics simulations, Angew. Chem., Int. Ed. Engl. 44 (2005) 1065–1067.

[51] N. Haspel, D. Zanuy, B. Ma, H. Wolfson, R. Nussinov, A comparative study of amyloid fibril formation by residues 15–19 of the human calcitonin hormone: a single beta-sheet model with a small hydrophobic core, J. Mol. Biol. 345 (2005) 1213–1227.

[52] J.T. Guo, R. Wetzel, X. Ying, Molecular modeling of the core of A beta amyloid fibrils, Proteins-Struct. Funct. Bioinform. 57 (2004) 357–364.

[53] B. Urbanc, L. Cruz, S. Yun, S.V. Buldyrev, G. Bitan, D.B. Teplow, H.E. Stanley, In silico study of amyloid beta-protein folding and oligomerization, Proc. Natl. Acad. Sci. U. S. A. 101 (2004) 17345–17350.

[54] I. Daidone, F. Simona, D. Roccatano, R.A. Broglia, G. Tiana, G. Colombo, A. Di Nola, Beta-hairpin conformation of fibrillogenic peptides: structure and alpha-beta transition mechanism revealed by molecular dynamics simulations, Proteins 57 (2004) 198–204.

[55] N.V. Buchete, G. Hummer, Structure and dynamics of parallel beta-sheets, hydrophobic core, and loops in Alzheimer's A beta fibrils, Biophys. J. 92 (2007) 3032–3039.

[56] N.V. Buchete, R. Tycko, G. Hummer, Molecular dynamics simulations of Alzheimer's beta-amyloid protofilaments, J. Mol. Biol. 353 (2005) 804–821.

[57] D.K. Klimov, D. Thirumalai, Dissecting the assembly of Abeta16–22 amyloid peptides into antiparallel beta sheets, Structure (Camb.) 11 (2003) 295–307.

[58] S. Tomaselli, V. Esposito, P. Vangone, N.A. van Nuland, A.M. Bonvin, R. Guerrini, T. Tancredi, P.A. Temussi, D. Picone, The alpha-to-beta conformational transition of Alzheimer's Abeta-(1–42) peptide in aqueous media is reversible: a step by step conformational analysis suggests the location of beta conformation seeding, ChemBioChem 7 (2006) 257–267.

[59] M.L. DeMarco, V. Daggett, From conversion to aggregation: protofibril formation of the prion protein, Proc. Natl. Acad. Sci. U. S. A. 101 (2004) 2293–2298.

[60] A. Barducci, R. Chelli, P. Procacci, V. Schettino, Misfolding pathways of the prion protein probed by molecular dynamics simulations, Biophys. J. 88 (2005) 1334–1343.

[61] L. Esposito, C. Pedone, L. Vitagliano, Molecular dynamics analyses of cross-{beta}-spine steric zipper models: {beta}-sheet twisting and aggregation, Proc. Natl. Acad. Sci. U. S. A. 103 (2006) 11533–11538.

[62] F. Ding, J.M. Borreguero, S.V. Buldyrey, H.E. Stanley, N.V. Dokholyan, Mechanism for the alpha-helix to beta-hairpin transition, Proteins 53 (2003) 220–228.

[63] D. Peretz, R.A. Williamson, Y. Matsunaga, H. Serban, C. Pinilla, R.B. Bastidas, R. Rozenshteyn, T.L. James, R.A. Houghten, F.E. Cohen, S.B. Prusiner, D.R. Burton, A conformational transition at the N terminus of the prion protein features in formation of the scrapie isoform, J. Mol. Biol. 273 (1997) 614–622.

[64] H. Mihara, Y. Takahashi, A. Ueno, Design of peptides undergoing self-catalytic alpha-to-beta transition and amyloidogenesis, Biopolymers 47 (1998) 83–92.

[65] L. Kalé, R. Skeel, M. Bhandarkar, R. Brunner, A. Gursoy, N. Krawetz, J. Phillips, A. Shinozaki, K. Varadarajan, K. Schulten, NAMD2: greater scalability for parallel molecular dynamics, J. Comput. Phys. 151 (1999) 283–312.

[66] A.D. MacKerell Jr., D. Bashford, M. Bellott, R.L. Dunbrack Jr., J.D. Evanseck, M.J. Field, S. Fischer, J. Gao, H. Guo, S. Ha, D. Joseph-McCarthy, L. Kuchnir, K. Kuczera, F.T.K. Lau, C. Mattos, S. Michnick, T. Ngo, D.T. Nguyen, B. Prodhom, W.E. Reiher III, B. Roux, M. Schlenkrich, J.C. Smith, R. Stote, J. Straub, M. Watanabe, J. Wiórkiewicz-Kuczera, D. Yin, M. Karplus, All-atom empirical potential for molecular modeling and dynamics studies of proteins, J. Phys. Chem., B 102 (1998) 3586–3616.

[67] C.A. MacRaild, G.J. Howlett, P.R. Gooley, The structure and interactions of human apolipoprotein C-II in dodecyl phosphocholine, Biochemistry 43 (2004) 8084–8093.

[68] W.L. Jorgensen, J. Chandrasekhar, J.D. Madura, R.W. Impey, M.L. Klein, Comparison of simple potential functions for simulating liquid water, J. Chem. Phys. 79 (1983) 926–935.

[69] T.E. Cheatham, J.L. Miller, T. Fox, T.A. Darden, P.A. Kollman, Molecular-dynamics simulations on solvated biomolecular systems — the Particle Mesh Ewald Method leads to stable trajectories of DNA, RNA, and proteins, J. Am. Chem. Soc. 117 (1995) 4193–4194.

[70] W.L. DeLano, The PyMOL Molecular Graphics System DeLano Scientific, San Carlos, CA, USA, , 2002 http://www.pymol.org.

[71] D. Frishman, P. Argos, Knowledge-based protein secondary structure assignment, Proteins 23 (1995) 566–579.

[72] W. Humphrey, A. Dalke, K. Schulten, VMD — visual molecular dynamics, J. Mol. Graph. 14 (1996) 33–38.

[73] M. Feig, A.D. MacKerell, C.L. Brooks, Force field influence on the observation of pi-helical protein structures in molecular dynamics simulations, J. Phys. Chem., B 107 (2003) 2831–2836.

[74] F.S. Legge, A. Budi, H. Treutlein, I. Yarovsky, Protein flexibility: multiple molecular dynamics simulations of insulin chain B, Biophys. Chemist. 119 (2006) 146–157.

[75] M.N. Fodje, S. Al-Karadaghi, Occurrence, conformational features and amino acid propensities for the pi-helix, Protein Eng. 15 (2002) 353–358.

[76] R. Armen, D.O. Alonso, V. Daggett, The role of alpha-, 3(10)-, and pi-helix in helix→coil transitions, Protein Sci. 12 (2003) 1145–1157.

[77] M. O'Donohue, E. Minasian, S.J. Leach, A.W. Burgess, H.R. Treutlein, PEPCAT — a new tool for conformational analysis of peptides, J. Comput. Chem. 21 (2000) 446–461.

[78] P.N. Lewis, F.A. Momany, H.A. Scheraga, Chain reversals in proteins, Biochim. Biophys. Acta 303 (1973) 211–229.

[79] J.S. Richardson, The anatomy and taxonomy of protein structure, Adv. Protein Chem. 34 (1981) 167–339.

[80] G.D. Rose, L.M. Gierasch, J.A. Smith, Turns in peptides and proteins, Adv. Protein Chem. 37 (1985) 1–109.

[81] K.C. Chou, Prediction of tight turns and their types in proteins, Anal. Biochem. 286 (2000) 1–16.

[82] O. Tcherkasskaya, W. Sanders, V. Chynwat, E.A. Davidson, C.S. Orser, The role of hydrophobic interactions in amyloidogenesis: example of prion-related polypeptides, J. Biomol. Struct. Dyn. 21 (2003) 353–365.

[83] M. Bucciantini, E. Giannoni, F. Chiti, F. Baroni, L. Formigli, J. Zurdo, N. Taddei, G. Ramponi, C.M. Dobson, M. Stefani, Inherent toxicity of aggregates implies a common mechanism for protein misfolding diseases, Nature 416 (2002) 507–511.

[84] M.J. Volles, S.J. Lee, J.C. Rochet, M.D. Shtilerman, T.T. Ding, J.C. Kessler, P.T. Lansbury Jr., Vesicle permeabilization by protofibrillar alpha-synuclein: implications for the pathogenesis and treatment of Parkinson's disease, Biochemistry 40 (2001) 7812–7819.

[85] G. Wei, N. Mousseau, P. Derreumaux, Complex folding pathways in a simple beta-hairpin, Proteins 56 (2004) 464–474.

[86] D.B. Volkin, H. Mach, C.R. Middaugh, Degradative covalent reactions important to protein stability, Mol. Biotechnol. 8 (1997) 105–122.

[87] J. Gao, D.H. Yin, Y. Yao, H. Sun, Z. Qin, C. Schoneich, T.D. Williams, T.C. Squier, Loss of conformational stability in calmodulin upon methionine oxidation, Biophys. J. 74 (1998) 1115–1134.

[88] J.L. Liu, K.V. Lu, T. Eris, V. Katta, K.R. Westcott, L.O. Narhi, H.S. Lu, In vitro methionine oxidation of recombinant human leptin, Pharm. Res. 15 (1998) 632–640.

[89] I. DalleDonne, A. Milzani, R. Colombo, The tert-butyl hydroperoxide-induced oxidation of actin Cys-374 is coupled with structural changes in distant regions of the protein, Biochemistry 38 (1999) 12471–12480.

[90] G. Bitan, B. Tarus, S.S. Vollers, H.A. Lashuel, M.M. Condron, J.E. Straub, D.B. Teplow, A molecular switch in amyloid assembly: Met35 and amyloid beta-protein oligomerization, J. Am. Chem. Soc. 125 (2003) 15359–15365.

[91] L. Hou, I. Kang, R.E. Marchant, M.G. Zagorski, Methionine 35 oxidation reduces fibril assembly of the amyloid abeta-(1–42) peptide of Alzheimer's disease, J. Biol. Chem. 277 (2002) 40173–40176.

[92] D.A. Butterfield, A.I. Bush, Alzheimer's amyloid beta-peptide (1–42): involvement of methionine residue 35 in the oxidative stress and neurotoxicity properties of this peptide, Neurobiol. Aging 25 (2004) 563–568.